The structure of Mediterranean arcs: new insights from the Calabrian Arc subduction system

Prada, M.[1], Ranero, C.R.[2], Sallares, V.[1], Grevemeyer, I.[3], Roberto de Franco[4], Gervasi., A.[5,6], Zitellini, N.[7]

(1) Barcelona-CSI, Inst. de Ciències del Mar-CSIC, Barcelona, Spain

(2) Barcelona-CSI, Inst. de Ciències del Mar, ICREA at CSIC, Barcelona, Spain

(3) GEOMAR Helmholtz Centre for Ocean Research Kiel, Germany

(4) Istituto di Geologia Ambientale e Geoingegneria IGAG-CNR, Milano, Italy

(5) Istituto Nazionale di Geofisica e Vulcanologia, Osservatorio Nazionale Terremoti, sede di Rende, Italy

(6) Dipartimento di Biologia, Ecologia e Scienze della Terra, Università della Calabria, Rende, Italy

(7) Istituto Scienze Marine ISMAR-CNR, Bologna, Italy

Abstract

The formation of Cenozoic mountain belts in the Mediterranean realm was preceded by tens of millions of years of subduction, forming volcanic arcs, and frontal contractional systems. In addition, subduction usually involves slab rollback and formation of oceanic backarcs. Although such structure must have influenced the orogeny of Mediterranean mountain belts, no active analog has been mapped with modern crustal-scale seismic methods. Here, we study the entire Calabrian subduction system to map the structure resulting from Tethys lithosphere subduction and slab roll back, in a process that must be akin to that operating during a phase of the formation of the Mediterranean orogenic belts. We present a crustal-scale cross section of the entire Calabrian subduction system

obtained from on- and off-shore wide-angle seismic data. The 2D P-wave velocity section shows spatially abrupt (< 5 km of profile distance) structural and petrological transitions from the Ionian sedimentary wedge and Calabrian arc, to the rifted NW Calabrian margin, where the Quaternary Aeolian arc is emplaced. The margin, then, transitions northwards into the Marsili backarc region, where exhumed mantle and localized volcanism occurred during its formation. This complex structure implies rapid temporal and spatial changes between magmatic and amagmatic processes, and between compressional and extensional regimes during the evolution of this subduction system. We find that some terranes involved in the Alpine orogeny share petrological and tectonic similarities with some domains of the Calabrian subduction system. Based on the results of this study we propose the Calabrian Arc system as an analog for the subduction structuration that preceded the formation of Alpine orogenic systems.

Keywords: Calabrian Arc, subduction; Mantle exhumation; Travel-time tomography; Wide-angle seismic data; Alpine orogeny; Mediterranean active arcs

1 Introduction

The Mediterranean realm includes a system of Cenozoic arcuate orogenic belts formed during the Alpine Orogeny (Dewey et al., 1973) (Fig. 1a). Mantle tomography images and plate reconstructions support that the collision events that formed these orogens were preceded by subduction of Tethys lithosphere (e.g. Dewey et al., 1973; Schettino and Turco, 2011). The evolution of the subduction systems must have often included slab retreat (e.g. Handy et al., 2010), causing the migration of volcanic arcs, extension of the overriding plate and formation of backarc basins possibly similar to the Tyrrhenian (Prada et al., 2015, Loreto et al., 2020) and the Alboran-South Balearic basins (Gomez de la Peña et al., 2018), and forearc contractional systems (e.g. Stampfli et al., 1998; Polonia et al., 2011; Marroni et al., 2017), determining thereby, the pre-collisional structuration of the lithosphere. The Gibraltar and Calabrian backarcs are no longer opening, and their domains are currently being inverted, which may indicate a current initial phase of a collision (Giaconia et al., 2015; Zitellini et al., 2020). Yet, the structure of Alpine-type belts has been associated to the imbrication of the domains formed during continental rifting (e.g. Reston and Manatchal 2011; Mohn et al., 2014), and the major lithospheric-scale structuration created during subduction has been largely ignored, possibly because of the fragmentary geological record in mountain belt that makes reconstructions disputable, and the lack of present-day potential analogs.

Reconstructing the structure of past subduction systems from present-day orogens is a challenging task because of the tectonic and metamorphic overprinting that terranes suffer during orogeny, and the incomplete outcrop information. An alternative way to infer such structure is by exploring the present-day subduction of the Tethys lithosphere in the Mediterranean, as occurs under the Calabrian, Gibraltar and Hellenic arcs (Fig. 1a)

(Spakman and Wortel, 2004; Müller et al., 2008). Possibly similar to Alpine subductions (e.g. Maffione and van Hinsbergen, 2018), the upper plate of these present-day subduction systems has been shaped by slab retreat, backarc opening, and accretionary forearc systems. Therefore, understanding of the forearc-to-backarc structure of present-day subduction systems in the Mediterranean may provide insights into the processes that shaped Alpine systems before collision.

In this work, we focus on the Calabrian subduction system, which includes the Tyrrhenian backarc basin, the Aeolian volcanic arc, the NW Calabrian margin, the Calabrian arc and the contractional Ionian wedge (Fig. 1a and 1b). Vintage (i.e. 1970) refraction studies provided 1D crustal velocity information across the subduction system, bringing first-order approximations on the crustal structure of the Calabrian arc (e.g. Cassinis et al., 2003). Regional earthquake tomography of the Calabrian region has provided insights on the structure of the slab and the petrological nature of the deep lithosphere and asthenosphere (e.g. Caló et al., 2009). However, these studies do not provide enough resolution to assess in detail the structure and petrological nature of shallow lithospheric domains (i.e. crust and uppermost mantle) across the subduction system.

To assess the forearc-to-backarc structure of this system, we present a detailed P-wave velocity (V_P) cross section of the entire subduction system using travel-time tomography from wide-angle seismic data (WAS) (Fig. 1) acquired in 2015 during the CHIANTI (Calabrian arc Hazards in IoniAN and TyrrhenIan seas) experiment (Fig. 1b). The 425 km-long model provides unprecedented information of the structure and petrology of shallow lithospheric domains across the Calabrian subduction system from the forearc to the backarc (Fig 1b).

2 The Calabrian Arc subduction system

Calabria has earthquakes activity up to ~500 km depth under the northern margin of Calabria, delineating a ~70^{o} NW dipping slab (Spakman and Wortel, 2004; Chiarabba et al., 2005). Slab rollback has been driving backarc basin formation by upper plate extension, similar to other regions of the Western and Central Mediterranean since the Oligocene (~30Ma; Malinverno and Ryan, 1986; Schettino and Turco, 2011). After the opening of the Liguro-Provençal basins, the east-southeast rollback of the Apennines-Calabrian subduction system initiated the Tyrrhenian backarc basin in the early Tortonian (~11 Ma) (Kastens and Mascle, 1990). During the Messinian (5.3-6 Ma) the potential under-thrusting of the continental lithosphere of Adria stopped slab rollback and backarc extension in the northern Tyrrhenian (Faccenna et al., 2001).

In contrast, the central and southern subduction front migrated towards the southeast (Spakman and Wortel, 2004), opening the central and southern Tyrrhenian Basin, and forming the Magnaghi and Vavilov basins during the Pliocene, and the Marsili basin during the Quaternary (Beccaluva et al., 1990; Kastens and Mascle, 1990) (Fig. 1b). Ocean Drilling Program (ODP) Leg 107 and Deep Sea Drilling Program (DSDP) Leg 42 recovered mid-ocean ridge basalts in the Magnaghi and Vavilov basins (Dietrich et al., 1977; Beccaluva et al., 1990). Further basalts were also sampled at the top of the basement in the Marsili basin (Kastens and Mascle, 1990) (Fig. 1b). Consequently, these basins have commonly been interpreted as regions where break up led to oceanic spreading. However, recent V_p models across the Vavilov and Magnaghi basins support that their basement is mainly composed of exhumed mantle rocks, and that basaltic ridges in the area are localized magmatic events (Prada et al., 2015, 2016). The occurrence of exhumed mantle in these two basins is further supported by the drilling of serpentinized peridotites

110 at ODP site 651(Bonatti et al., 1990) (Fig. 1b).

111 The southeastward migration of the subduction system resulted in rifting of the NW
112 Calabrian margin and emplacement of the Quaternary Aeolian volcanic arc at < 1.2 Ma
113 (Argnani and Savelli, 1999), the tectonic Calabrian Peninsula, formed by Paleozoic to
114 Eocene metamorphic rocks covered by Cenozoic sedimentary units (Vitale et al., 2019),
115 and the Ionian contractional wedge (Polonia et al., 2011) (Fig. 1a).

116 3 Acquisition, processing and picking of wide-angle seismic data

117 The CHIANTI seismic experiment was conducted onboard the Spanish R/V Sarmiento
118 de Gamboa. The offshore data used in this study were acquired along two offshore
119 profiles, WAS1 in the Ionian Sea, and WAS2 in the Tyrrhenian backarc region (Fig.1b).
120 The offshore data were recorded by 14 and 17 LC2000 Ocean Bottom Seismometers
121 (OBS) of the Spanish National Research Council (CSIC) along profiles WAS1 and
122 WAS2, respectively. OBS spacing along both lines was ~ 10 km. The seismic source was
123 generated by two arrays of 9 airguns each, which released a total volume of 4760 cu. in.
124 (78 l), and worked at 15 m of depth to provide a range of frequencies between 7-45 Hz,
125 optimum for crustal-scale WAS experiments. Shot interval along both lines was 90s
126 (~230 m at 5 knots). Land stations in Calabria were installed by the University of
127 Calabria. In this study, we use 31 OBS records with useful data and 3 out of the 5 land
128 stations installed in Calabria, which recorded the shots along both WAS1 and WAS2 (Fig.
129 1).

130 We relocated all OBSs using an in-house Metropolis-Hastings algorithm that minimizes
131 the misfit function between the observed and synthetic first arrival travel-times of the
132 water wave to find the most likely location of the OBS. We applied a bandpass filter (1-
133 5-18-25 Hz) to all seismic records to enhance the seismic signal and manually picked

travel-times of first arrival and critical reflections. In the contractional wedge, near offset (< 15 km) first arrival times from OBS record sections of profile WAS1 define a first refracted seismic phase with an apparent velocity of 3-4 km/s that corresponds to refracted P-waves through the shallow sedimentary sequence of the contractional wedge or P_s (Fig. 2a-b). Between 15-20 km offset a second refracted seismic phases with an apparent velocity of 5-6 km/s can be identified in those OBS deployed near the shore (Fig. 2b). We interpreted this latter phase as refracted P-waves through the uppermost basement of the contractional wedge or P_b. Some sections show a prominent critical reflection at 15-20 km of offset, defining the transition between refracted phases P_s and P_b (Fig. 2a-b). We interpreted this phase as P-waves reflected at the top of the acoustic basement or P_sP (Fig. 2a-b). The land record sections of line WAS1 only allowed the identification of seismic phases P_s and P_sP, up to ~40 km offset (Fig. 2h).

From SE to NW in the NW Calabrian margin, OBS records along line WAS2 display a first refracted seismic phase with apparent velocity of 6 km/s. This seismic phase is interpreted as a P-wave refracted within the crust (P_g). At further offset (> 40 km offset), we identified a second refracted phase, in this case with a faster apparent velocity of ~8 km/s. We interpret this phase as a P-wave refracted within the uppermost mantle (P_n). The transition from P_g to P_n is marked by the arrival of critical reflections at the crust-mantle boundary (P_mP). An additional reflected phase can be identified in some receivers located in the NW Calabrian margin. This seismic phase arrives at shorter offsets than P_mP's, at 30-20 km on average (P_gP in Fig. 2c), indicating the presence of a major intra-crustal interface below the margin. Towards the NW, in the Marsili basin, OBS receivers do not display clear P_g and P_mP phases, just a single prominent refracted phase with apparent velocity of ~8 km/s. These seismic records resemble to ocean bottom hydrophone data recorded in the exhumed mantle region of the Magnaghi and Vavilov

basins during the MEDOC WAS experiment (Prada et al., 2016). For layer-stripping modelling purposes, we also assigned this phase the P_n label. Land station records of line WAS2 show clear P_g and P_mP phases (Fig. 2g).

In total, we picked 2837 P_s, 857 P_sP and 170 P_b from WAS1 record sections, and 4378 P_g, 675 P_gP, 1090 P_mP, and 3081 P_n from WAS2 records. Picking uncertainty was set between 30 ms and 100 ms based on the amplitude ratio of a 250 ms-long window before and after the picked travel-time, following the approach of Zelt and Forsyth (1994).

4 Methods: travel-time tomography

We invert for V_p and the geometry of the different seismic interfaces (i.e. Moho) using the joint refraction and reflection travel-time tomography code TOMO2D (Korenaga et al., 2000). The starting velocity model is parameterized as a regular grid hanging from the seafloor, with 250 m node spacing both vertically and horizontally. Regularization parameters are defined by horizontal and vertical correlation lengths (CL) that increase from top to bottom in the velocity grid. In this study, we set 0.2 km and 1 km for the vertical and horizontal CL at the top of the model, respectively, and 10 km and 20 km at the bottom of the model, located at 50 km depth.

We have followed a layer-stripping strategy as in Prada et al. (2015) to resolve the sharp velocity contrast attributed to the top of the acoustic basement in the contractional wedge, and the crust-mantle boundary of the NW Calabrian margin. This way, along WAS1 we built the model following a two-step inversion, each step consisting of 10 iterations. In the first step, we inverted P_s and P_sP travel-times. The corresponding solution is included and damped in the starting model for the second step, in which we inverted P_b travel-times together with P_s, and P_sP travel-times. We followed a similar approach to build the

model along profile WAS2. First, P_g and P_mP travel-times were inverted to solve the V_p structure of the crust beneath the NW Calabrian margin, as well as the Moho geometry. In a second step, we included and damped the solution of the first inversion within the starting model for the second inversion step, in which we added P_n travel-times to the previous dataset. Once both models (i.e. WAS 1 and 2) were obtained, travel-times of refracted phases of land stations in both profiles were jointly inverted to better constrain the velocity structure of the Calabrian arc using crossing rays. P_gP travel-times along WAS2 were inverted using the final velocity model as a reference to retrieve the geometry and location of the intra-crustal reflector beneath the margin (Fig. 3). Acceptable ray coverage beneath profile WAS1 in the Ionian is restricted to the first 10 km of depth of the model, while tomographic constraints along WAS2 can reach down to 15-20 km of depth (Fig.3b). The final root mean square (RMS) of refracted and reflected travel-times for the final velocity model (Fig. 3) is ~60 ms and ~80 ms, respectively.

4.1 Uncertainty and resolution of the tomographic model

The uncertainty of the model parameters was assessed by means of a Monte Carlo analysis (e.g. Korenaga et al., 2000). We followed the same layer-stripping strategy used to obtain the preferred model to estimate the parameters uncertainty of each layer of the model. We tested 100 realizations, each of them using a 1D V_p-depth profile and a flat reflector as initial model, and a travel-time dataset perturbed with random Gaussian noise (up to ±100ms). To generate the starting model, we have applied a random perturbation of ±10% and ±6% for crustal and mantle velocities, respectively, of the reference velocity model for each layer (Supplementary Table 1). A perturbation of ±4 km respect the reference depth for each reflector was applied to generate each starting interface (Supplementary Table 1). The set of correlation lengths were also randomly perturbed in

each realization. This way, we have used for each CL: 3±2 for the top horizontal CL, 15±5 for the bottom horizontal CL, 0.3±0.2 for the top vertical CL, and 4±1 for the bottom vertical CL.

All realizations converge after 20 iterations with an overall RMS of travel-times of 80 ms (Fig. 4a). We have computed the standard deviation of V_p and depth of each reflector to quantify the range of variation (uncertainty) attributed to all random errors. These values show that the model presents standard deviations < ±0.1 km/s in most of the model, indicating a satisfactory control of seismic velocities. As expected, higher values (±0.2 - ±0.3 km/s) are observed in regions with a sharp vertical velocity contrast or limited ray coverage, like at the lower part of the wedge (Fig. 4). The uncertainty of each reflector ranges between ± 0.15 km in areas well covered by reflected rays, and ±4 km towards the edges of each reflector, where ray coverage is limited (Fig. 3b).

We have also evaluated the resolution of the tomographic model by performing a checkerboard test, following the approach in Zelt (1998). This way, a total of 72 checkerboard-type models with nine different squared cell sizes (4, 6, 8, 10, 12, 14, 16, 18, and 20 km), and with a maximum velocity perturbation of 5% have been tested. For each cell size, eight different patterns were created with positive and negative polarity, with and without 45º rotation, and with and without a diagonal shift of half of the cell size. Each checkerboard pattern was added to the preferred tomographic model to create each target model and compute the synthetic travel-times. Before inverting each synthetic dataset, we added a random Gaussian noise, with a standard deviation corresponding to the picking uncertainty, to each travel-time, as in the Monte Carlo analysis.

After inverting each dataset using the preferred model as starting model, we compute the semblance between the retrieved pattern and the corresponding target pattern. As in Zelt

(1998), we consider the pattern to be well retrieved for a semblance > 0.7 (red contour Fig. 5a and 5b). We then compute the average semblance for each cell size and combine them all in a resolution map that depicts the maximum resolution depth of each cell size (Fig. 5c). The map shows that the minimum cell size that can be retrieved is 4 km along profile WAS2, while it is 6 km along WAS1. The resolution depth of the largest cell size (20 km) ranges between 15-20 km of depth beneath the arc/backarc, and 10 km of depth beneath the contractional wedge. The differences in resolution between the arc/backarc and the wedge is caused by the lower amount of travel-times (rays) observed in the seismic records of the Ionian region (Fig. 3b).

5 Results

From SE to NW, the final tomographic model shows the V_p structure of the main crustal domains of the Calabrian subduction system, namely the Ionian contractional wedge, the Calabrian Arc, the NW Calabrian rifted margin, the volcanic arc (at ~290 km in Fig. 3), and the Marsili backarc basin in the Tyrrhenian (Fig. 3).

In the Ionian, the V_p model delineates the Pre-Messinian wedge towards Calabria, across the Inner Plateau and the Squillace basin (Fig. 1b and 3). The shallow velocity structure across the Pre-Messinian and Inner Plateau sectors, which have distinct seafloor morphology, indicates a continuous crustal domain. The V_p of the shallowest ~3 km displays a gradual increase towards the coast (km 0-175 in figure 3a). V_p of <~3 km/s correspond to low consolidated sediment, particularly thick under OBSs 7-6, 3, and 1 (Fig. 3). The shallow V_p structure in the wedge has good ray coverage (Fig 3b) and uncertainties <0.1 km/s (Fig. 4), with well-resolved lateral changes of ~10 km in width (Fig. 5). Underneath, V_p steadily increases from 4.0 km/s to 5.0-6.0 km/s with depth (Fig 3a). V_p >~4 km/s imply a well consolidated material, and V_p 5.0-6.5 km/s at 10-15 km

depth indicate crystalline rocks with little porosity (Fig. 3), although with depth ray coverage and resolution decrease and uncertainty increases (fig. 4). Near the coast, the ~4-5 km deep Squillace basin (beneath OBS 17-16 in Fig. 3) V_p increases from 1.70 to 4.0-4.5 km/s at 6-7 km depth, underlaid by V_p > 5 km/s that supports shallow continental basement rocks. A relatively continuous intra-wedge regional wide-angle reflector roughly follows V_p 3-3.5 km/s, shallowing from 10 km depth beneath OBS 17 to ~5 km depth beneath OBS 7-4. The V_p does not abruptly changes across the reflector, which may indicate a rapid decrease in porosity and/or fracturing with depth rather than an abrupt boundary.

The structure beneath mainland Calabria is partially resolved with rays from both Ionian and Tyrrhenian marine shots. V_p increases from ~4.0-4.5 km/s at ~1 km depth to 6.5-7 km/s at 20-22 km depth, above the Moho mapped by P_mP reflections in a sector of NW Calabria (at 220 km in Fig. 3). These values are in agreement with Moho depth from the 1979 Calabria transect (Cassinis et al., 2003), and receiver functions (Piana-Agostinetti et al 2009). The Calabria crust V_p range and low vertical velocity gradient (~0.1 s^{-1}) match typical continental crystalline crust V_p distribution (Christensen and Mooney, 1995) as shown in Fig. 6.

The NW Calabria rifted margin continental crust thins from ~20 km under the coastline to 10 km at the NW edge (km ~325 in Fig. 3). Along this margin, V_p increases from 1.8 km/s to 3.5 km/s at ~1.5 km below seafloor and then abruptly to 5.0 km/s at 2 km below seafloor roughly marking the basement top (Fig. 3). The basement V_p is laterally homogeneous and with a gentle vertical gradient from ~ 5 to ~7.0 km/s near the Moho. An intra-basement reflector delineates a slight decrease in vertical gradient for V_p >5.7-6.0. The basement velocity under Lametini volcano of the Aeolian arc (Fig. 1b) is well-

278 constrained and comparatively higher, of 6 km/s at ~1 km beneath top basement to ~7.0-
279 7.3 km/s in the lowermost crust (km ~290 in Fig. 3). The margin uppermost mantle V_p
280 increases from 7.7-7.8 km/s to 8.2 km/s in 5 km under the Moho (Fig. 3).

281 The backarc region displays an abrupt lateral change in V_p structure at km ~330 (Fig 3a).
282 The Marsili basin has no Moho boundary (no P_mP reflections, Fig. 2e-f) and the transition
283 to mantle V_p occurs with comparatively steep vertical velocity gradients of ~1 s^{-1} for V_p
284 of ~4.5-7.0 km/s reaching V_p ~ 7.5-8.0 km/s at ~5 km below seafloor. The general Marsili
285 basin V_p structure is locally interrupted by a gentler vertical velocity gradients of the two-
286 layer V_p structure under the 3-km-high Marsili volcano. The upper layer increases rapidly
287 from 3 km/s near the surface to 6 km/s at 6-7 km of depth, with a 0.6 s^{-1} gradient (Fig. 3).
288 The second layer V_p increases from 6 km/s to ~8 km/s with a 0.2 s^{-1} gradient (Fig. 3). The
289 V_p model beneath small seafloor ridges under OBS 28 and 29 contains local sub-vertical
290 anomalies with relatively lower V_p (Fig 1 and 3).

291 6 Discussion

292 6.1 Geological interpretation

293 6.1.1 Ionian wedge

294 The upper 4-5 km of the internal wedge is characterized by low velocity regions (i.e. <
295 2.5 km/s). These low velocity anomalies may indicate comparatively higher porosity in a
296 region of fluid overpressure. Some of these low velocity anomalies (i.e. OBS 6-7 in Fig.
297 1 and 3) are spatially coincident with mud volcanoes mapped with multibeam bathymetry
298 (Gutscher et al. 2017). that are associated with fluid and mud expulsion (Loher et al.,
299 2018). Previous tectonic interpretation based on MCS data shows that low velocity
300 anomalies beneath OBS 6 to 1 are spatially coincident with compressional structures

(Polonia et al., 2011) (Fig. 1b). Thus, we interpret that these low velocities may indicate regions of the wedge where active shortening is causing fluid outflow through thrust faulting.

6.1.2 The NW Calabrian margin

The basement of the NW Calabrian margin and that beneath Calabrian exhibits a similar vertical V_p profile than the global continental crust compilation of Christensen and Mooney (1995) (Fig. 3 and 6). The Moho beneath the NW Calabrian margin shallows from 20-22 km of depth beneath Mainland to ~10 km of depth, reflecting the result of the Late Miocene backarc extension of the margin (~11-7 Ma ago; Kastens and Mascle, 1990).

The intra-crustal reflector modeled at 7-8 km depth roughly delineates the V_p ~5.8-6.0 km/s (Fig. 3). The boundary does not mark an abrupt change either in Vp or in gradient with depth, and we speculate that it may represent a transition with depth in rock fracturing and associated fluid percolation, possibly related to a change from shallower fault-controlled brittle deformation to deeper plastic lower crust deformation. A similar result is found in the Galicia Interior basin (Perez-Gussinyé et al., 2003), where the resulting reflector delineate the 6.2-6.3 km/s V_p at 9-10 km depth in a ~15-km-thick basement. There, coincident seismic images and thermal modelling support that the reflector marks the boundary between a faulted upper crust and a ductile lower crust at the time of rifting.

6.1.3 The volcanic arc

The NW Calabrian margin is characterized by V_p > 7 km/s beneath the volcanic arc (Fig .3). These velocities are anomalously high for extended continental crust settings, which typically range between 6.69-6.93 km/s (Christensen and Mooney, 1995). To assess the

petrological nature of these rocks, we compare the vertical velocity structure of the Aeolian arc with (1) the vertical V_p structure of the NW Calabrian margin at 275 km of profile distance, (2) the empirical V_p-depth distribution of different rock-types of the Izu-Bonin-Mariana arc in the Pacific (Kitamura et al., 2003), and (3) the V_p-depth reference function for continental crust (Christensen and Mooney, 1995) (Fig. 3a). The V_p-depth distribution of the arc reveals a compositional differentiation from felsic/intermediate (i.e. 6.0 to 6.8 km/s; Christensen and Mooney, 1995) in the upper crust to mafic material in the lower crust (Fig. 3a), where the V_p-depth distribution coincides with the V_p-depth distribution for gabbroic rocks of Izu-Bonin-Mariana arc (Fig. 6a; Kitamura et al., 2003).

6.1.4 Marsili backarc basin

In the backarc region we compared average vertical velocity distribution at either side of the Marsili volcano, with reference V_p-depth functions from modern tomographic studies for oceanic crust (Grevemeyer et al., 2018a), exhumed mantle regions from the central Tyrrhenian and Gulf of Cadiz (Prada et al., 2015), as well as exhumed mantle regions from ultra-slow spreading centers (Grevemeyer et al., 2018b). Oceanic crust and exhumed mantle references have different V_p-depth trends reflecting their petrology (Fig. 6b). The oceanic crust reference has two-layer structure associated to the petrological differentiation between the widespread basaltic layer 2 and the gabbroic layer 3 (e.g. Grevemeyer et al., 2018a), while the exhumed mantle field appears as a continuous, comparatively steeper velocity gradient of 0.6-0.7 s^{-1} of the upper ~5-6 km of basement, reflecting the decreasing degree of serpentinization with depth (e.g. Prada et al., 2016). The comparison with our observations supports that the basement of the Marsili backarc basin is made of exhumed mantle similar to the Magnaghi and Vavilov basins in the Tyrrhenian.

Previous regional studies interpreted that the Marsili basin is floored by oceanic crust produced by ultrafast oceanic spreading (e.g. Nicolosi et al., 2006; Manu-Marfo et al., 2019). However, our results show that the structure that can be related to oceanic spreading, that is the Marsili volcano and neighboring ridges, are isolated velocity anomalies in the tomographic model, and that the bulk of the basin has a velocity gradient matching the exhumed mantle V_P-depth reference. This result, together with similar observations from the Magnaghi and Vavilov basins (Prada et al., 2016), indicate that mantle exhumation and emplacement of localized oceanic ridges and large-volcanic edifices (Fig.1b) have been recurrent events during the opening of the Tyrrhenian backarc.

The occurrence of exhumed mantle in the Tyrrhenian basins results paradoxical. Stratigraphic record analysis of the Marsili Basin allowed to infer that the basin opened ~2 Ma ago (Kastens and Mascle et al., 1990; Argnani and Savelli, 1999), so that mantle exhumation should have occurred at a rate of 3.5-4.5 cm/yr (Kastens and Mascle et al., 1990), although magnetic anomaly analysis suggests a much faster rate (~19 cm/yr; Nicolosi et al., 2006). This rate is exceptionally fast considering models of partial decompression melting, which suggest that mantle unroofing should not occur at rates >~2 cm/yr (e.g. Grevemeyer et al., 2018b). Geochemical analyses of serpentinzed peridotites from site 651 show that these rocks are strongly depleted in lithophile elements during recurrent partial melting events (Bonatti et al., 1990). This suggests the presence of a depleted mantle source, which could restrict the production of partial decompression melting during lithospheric extension (Perez-Gussinyé et al., 2006).

6.2 The forearc-to-backarc structure of the Calabrian arc: resemblance with Alpine subduction systems

The 450 km long transect displays the contrasting V_p structures of the Ionian contractional wedge, the 20-22 km thick continental crust of the Calabrian Arc, the NW Calabrian rifted margin, locally modified by ~20 km-wide volcanic arc activity, and the exhumed mantle domain of the Marsili backarc basin, locally intruded by volcanic ridges (Fig. 7). These domains represent terranes made of distinct petrological suites and formed by contrasting deformation regimes, bounded by <4-5 km wide transitions , near the resolution limit of our data (Fig. 5). This complex terrane structuration involves a tectonic and magmatic evolution not fully understood. The NW Calabrian margin integrates the evolution of extended continental crust possibly by a Miocene to younger rift (Kastens and Mascle et al., 1990), modified by the emplacement of the volcanic arc, and the development of the Plio-Quaternary Paola basin, currently in a forearc position, with up to 5 km infill (Zitellini et al., 2020) that extends towards the NW of our transect (Fig. 1 and 3). The backarc Marsili basin is possibly Quaternary (Kastens and Mascle et al., 1990), and formed by amagmatic extension leading to mantle exhumation and the subsequent intrusion of a ~20 km-wide volcano and localized ridges. This basin is surrounded to the north, east and south by continental crust and volcanic complexes related to the subduction (Fig 1b), while towards the northwest, the basin leads to the Vavilov Basin, where exhumed mantle and localized oceanic ridges were emplaced during its formation (Prada et al., 2016).

This complex structuration resulted from subduction and rollback of the Jurassic Tethys lithosphere, which is the same geodynamic process that controlled the subduction phase of possibly many Alpine systems (e.g. Schmid et al. 1996; Wortel and Spakman, 2000; Maffione and van Hinsbergen, 2018). The complex structure of the Calabrian subduction

system is possibly not unique or anomalous, and similarly complex structures might have occurred at overriding plates of ancient Alpine subduction systems.

General proposals indicate that the structural inheritance of rifted margin architecture is key to explain orogenic configuration (e.g. Reston and Manatchal 2011). More specifically Alpine rock units originally from the Jurassic Tethys (Froitzheim and Eberli 1990) are interpreted to signify a structural inheritance that significantly influenced the orogenic development of Alpine belts (e.g. Mohn et al., 2014). Based on those concepts, it is proposed that closure of suspected narrow oceans lacks significant subduction-related magmatism, leaving little trace in mountain belts like the Alps and Pyrenees. It is argued that those orogens develop fundamentally by processes in which the original rifted margins structure controls the final orogen architecture (e.g. Chenin et al., 2017). Although the Pyrenees are overwhelmingly interpreted as the closure of a narrow rifted basin, the Alps are debated and the subduction phase may have lasted 25 Ma, from Early Paleocene to at least Late Eocene, with >500 km of subduction (Schmid et al., 1996), similar to the present-day subduction systems in the Central Mediterranean (e.g. Faccenna et al., 2001). Therefore, such subduction system could have created a structuration similar to the Calabrian Arc system. Furthermore, at a larger scale, opening during Tethys-Ionian slab subduction and rollback since ~25 Ma triggered the formation of the passive margin of the Gulf of Lions, the Ligurian basin and the Corsica-Sardinia continental block (Schettino and Turco, 2011), which adds further complexity to a pre-collision scenario.

The geological record of several Alpine-type mountain belts retain unequivocal evidence of terranes formed during subduction , sharing similarities with domains of the Calabrian arc. Conspicuous units found in Alpine belts such as the Apennines, Alps, Hellenides, Dinarides, and Taurides are the remnants of forearc accretionary systems (e.g. Stampfli

et al., 1998; Okay et al., 2006; Marroni et al., 2017; Maffione and van Hinsbergen, 2018), and volcanic arcs (Sharkov et al., 2014). But the most distinctive units implying subduction are serpentinized mantle rocks accompanied by basaltic rocks found in Alpine-type ophiolites (e.g. Moghadam and Stern, 2015). Although some mantle rocks from the Alps are related to mantle exhumation in Tethys rift context (e.g. Froitzheim and Eberli 1990), the majority of these ophiolites have geochemical signatures that support a supra-subduction origin and are spatially associated to magmatic rocks with Island arc affinity (e.g. Dilek 2003; Moghadam and Stern, 2015; Maffione and van Hinsbergen, 2018), similar to Tyrrhenian samples (Beccaluva et al., 1990). In particular, assemblages similar to Tyrrhenian serpentinized mantle rocks are described in the east and west Vardar Ophiolites in Albania (Maffione and van Hinsbergen, 2018), the Tsiknias ophiolites in Greece (Lamont et al., 2020), and Iran (Moghadam and Stern, 2015). This latter suit of serpentinized mantle rocks found in Mesozoic ophiolites, formed prior to the construction of the Zagros belt, share a peridotite spinel composition with Tyrrhenian peridotites drilled at ODP leg 107 (Fig. 1). Both rocks present high values of Cr# (> 40) and low values of Mg# (< 60), indicating a similar degree of depletion during melt extraction at convergent margins (see fig. 7 in Bonatti et al., 1990; fig. 13 in Moghadam and Stern, 2015).

Based on these observations, it is likely that the pre-collisional structure of many Alpine orogens from South Europe to the Middle East that experienced extended subduction periods, possibly accompanied by slab retreat, was formed by neighboring terranes with distinct petrological and tectonic characteristics separated by spatially abrupt boundaries, resembling to the structuration mapped here across the of the Calabrian Arc (Fig. 7).

7 Conclusions

The first modern WAS transect across the Calabrian Arc system provides a 2D V_p tomographic image of the entire system along 450 km from forearc to the backarc region from joint inversion of refracted and reflected P-wave travel-times.

The Calabrian system structure is characterized by spatially abrupt changes (<4-5 km width) between domains formed by different processes and differing petrological and tectonic structures.

The frontal region where contractional tectonics dominate includes the offshore internal wedge formed mainly by consolidated rocks covered by 1-3 km of sediment with V_p < 3.5 km/s. The V_p model of the wedge displays gentle undulations defining local low velocity anomalies (< 2.5 km/s) suggesting the presence of high porosity regions of the wedge. These anomalies are spatially coincident with thrusting and mud volcanism on surface, suggesting that thrusting leads to fluid outflow to the seafloor. The transition between the inner wedge and Calabria occurs under the Squillace basin, with an abrupt shoaling of the consolidated basement rocks.

The Calabrian Peninsula has a 20-22 km thick crust with a typical continental crust velocity structure. The continental Calabrian crust was extended and thinned in the Miocene to 16-9 km across ~100 km of the NW Calabrian margin. The rifted margin structure was subsequently modified during Plio-Quaternary time by magmatic arc activity across a ~20 km wide area and the development of the 3-5 km thick Paola forearc basin. The continental crust abruptly thins over ~5 km width to the Marsili basin.

The 200 km wide Marsili basin has a vertical velocity gradient typical of exhumed mantle domains, similar to Vavilov and Magnani basins in the central Tyrrhenian. Local velocity

anomalies under Marsili volcano and low ridges indicate that basaltic features are isolated intrusions in the basement of the basin, which is inferred to be composed by serpentinized peridotite.

Although it has been long speculated that orogen formation is strongly influenced by the inherited structure of rifted continental margins, most conceptual models and reconstructions have not accounted for the subduction phase that possibly preceded collision in most of the Alpine-type orogens from South Europe to the Middle East. We show the first detailed structure of an analog of a system created by Tethys slab subduction and rollback, which has created an unanticipated complex pattern of large-scale lithospheric domains, some of which are similar to terranes found in Alpine-type mountain belts.

8 Acknowledgments

We would like to thank the science party of the CHIANTI survey. Special thanks to R/V Sarmiento de Gamboa officers and crew and the Marine Technology Unit of Spanish National Research Council (CSIC) and GEOMAR technicians. Thanks I. Guerra, R.L. Festa, G. Caielli, and A. Corsi for helping with deployment, and processing of landstation data. The CHIANTI survey was part of the HADES project funded by the Spanish MINECO (Ref # CTM2011-30400-C01 and CTM2011-30400-C02). We thank the editor John P. Brodholt and two anonymous reviewers for helping to improve previous versions of the manuscript. M. Prada is funded by the Beatriu de Pinós postdoctoral programme of the Government of Catalonia's Secretariat for Universities and Research of the Ministry of Economy and Knowledge (Ref # .2017BP00170). Thanks to Pierre Arroucau for his assistance during the development of the OBS relocation code. Special thanks to Carlos J. Garrido for fruitful discussion on the provenance of backarc exhumed mantle rocks.

Finally, thanks to Nicola Piana-Agostinetti for providing the location of earthquakes in Figure 1b and 8. Generic Mapping Tools (Wessel and Smith, 1995) was used in the preparation of this manuscript. This is a contribution of the Barcelona Center for Subsurface Imaging that is a Grup de Recerca de la Generalitat de Catalunya (2017 SGR 1662).

9 References

Argnani, A., & Savelli, C. (1999). Cenozoic volcanism and tectonics in the southernTyrrhenian sea: Space-time distribution and geodynamicsignificance. Journal of Geodynamics, 4(27), 409-432.

Beccaluva, L., E. Bonatti, C. Dupuy, et al. (1990), Geochemistry and mineralogy of volcanic rocks from the ODP Sites 650, 651, 655 and 654 in the Tyrrhenian Sea, In Kastens, K.A., Mascle, J., et al. (Eds.), Proceedings of the Ocean Drilling Program, Scientific Results 107, pp. 49– 74.

Bonatti, E., M. Seyler, J. Channell, J. Girardeau, and G. Mascle (1990), Peridotites drilled from the Tyrrhenian Sea, ODP Leg 107, In Kastens, K.A., Mascle, J., et al. (Eds.), Proceedings of the Ocean Drilling Program, Scientific Results 107, pp. 37– 48.

Caló, M., Dorbath, C., Luzio, D., Rotolo, S. G., & D'anna, G. (2009). Local earthquake tomography in the Southern Tyrrhenian region of Italy: Geophysical and petrological inferences on the subducting lithosphere. In Subduction Zone Geodynamics (pp. 85-99). Springer, Berlin, Heidelberg.

Cassinis R., Scarascia S., Lozej A., (2003), The deep crustal structure of Italy and surrounding areas from seismic refraction data. A new synthesis. Boll. Soc. Geol. Italiana, 122, 365-376.

Chenin, P., Manatschal, G., Picazo, S., Müntener, O., Karner, G., Johnson, C., and Ulrich, M., (2017). Influence of the architecture of magma-poor hyperextended rifted margins on orogens produced by the closure of narrow versus wide oceans: Geosphere, v. 13, no. 2,

p. 559–576, doi:10.1130 /GES01363.1.

Chiarabba, C., Jovane, L., & DiStefano, R. (2005). A new view of Italian seismicity using 20 years of instrumental recordings. Tectonophysics, 395(3-4), 251-268.

Christensen, N., and Mooney, W. (1995), Seismic velocity structure and composition of the continental crust: a global view, J. Geophys. Res, 100 (B7), doi:10.1029/95JB00259.

Colantoni P., A. Fabbri, P. Gallignani, R. Sartori, and J.P. Rehault, (1981) Carta Litologica e Stratigrafica dei Mari Italiani, scala 1/1.500.000, Litografia Artistica Cartografica,Firenze, Italy.

Dewey, J. F., Pitman III, W. C., Ryan, W. B., & Bonnin, J. (1973). Plate tectonics and the evolution of the Alpine system. Geological society of America bulletin, 84(10), 3137-3180.

Dietrich, V., R. Emmermann, J. Keller, and H. Puchelt (1977), Tholeitic basalts from the Tyrrhenian sea floor, Earth Planet. Sci. Let., 36, 285-296.

Dilek, Y. (2003). Ophiolite concept and its evolution. Special Papers-Geological Society of America, 1-16.

Faccenna, C., T.W. Becker, F. P. Lucente, L. Jolivet, and F. Rossetti (2001), History of subduction and backarc extension in the Central Mediterranean, Geophys. J. Int., 145, 809-820.

Froitzheim, N., & Eberli, G. P. (1990). Extensional detachment faulting in the evolution of a Tethys passive continental margin, Eastern Alps, Switzerland.Geological society of America bulletin, 102(9), 1297-1308.

Giaconia, F., Booth-Rea, G., Ranero, C. R., Gràcia, E., Bartolome, R., Calahorrano, A., Lo Iacono, C., Vendrell, M. G., Cameselle, A. L., Costa, S., Gómez de la Peña, L., Martínez-Loriente, S., Perea, H., and Viñas, M. (2015), Compressional tectonic inversion of the Algero-Balearic basin: Latemost Miocene to present oblique convergence at the Palomares margin (Western Mediterranean). Tectonics, 34, 1516– 1543. doi: 10.1002/2015TC003861.

Gomez de la Pena, L., Ranero, C. R., & Gràcia, E. (2018). The crustal domains of the Alboran Basin (western Mediterranean). Tectonics, 37(10), 3352-3377.

Grevemeyer, I., Ranero, C. R., & Ivandic, M. (2018a). Structure of oceanic crust and serpentinization at subduction trenches. Geosphere, 14(2), 395-418.

Grevemeyer, I., Hayman, N. W., Peirce, C., Schwardt, M., Van Avendonk, H. J., Dannowski, A., & Papenberg, C. (2018b). Episodic magmatism and serpentinized mantle exhumation at an ultraslow-spreading centre. Nature Geoscience, 11(6), 444-448.

Gutscher, M. A., Kopp, H., Krastel, S., Bohrmann, G., Garlan, T., Zaragosi, S., ... & Sallarès, V. (2017). Active tectonics of the Calabrian subduction revealed by new multi-beam bathymetric data and high-resolution seismic profiles in the Ionian Sea (Central Mediterranean). Earth and Planetary Science Letters, 461, 61-72. https://doi.org/10.1016/j.epsl.2016.12.020

Handy, M. R., Schmid, S. M., Bousquet, R., Kissling, E., & Bernoulli, D. (2010). Reconciling plate-tectonic reconstructions of Alpine Tethys with the geological–geophysical record of spreading and subduction in the Alps. Earth-Science Reviews, 102(3-4), 121-158.

Kastens, K., and Mascle, J. (1990), The geological evolution of the Tyrrhenian Sea: an introduction to the scientific results of ODP LEG 107, In Kastens, K.A., Mascle, J., et al. (Eds.), Proceedings of the Ocean Drilling Program, Scientific Results 107, pp. 3-26. doi:10.2973/odp.proc.sr.107.187.1990

Kitamura, K., Ishikawa, M., & Arima, M. (2003). Petrological model of the northern Izu–Bonin–Mariana arc crust: constraints from high-pressure measurements of elastic wave velocities of the Tanzawa plutonic rocks, central Japan. Tectonophysics, 371(1-4), 213-221

Korenaga, J., W. S. Holbrook, G. M. Kent, P. B. Kelemen, R. S. Detrick, H.-C. Larsen, J. R. Hopper, and T. Dahl-Jensen (2000), Crustal structure of the southeast Greenland margin from joint refraction and reflection seismic tomography, J. Geophys. Res., 105(B9), 21, 591–21, 614, doi:10.1029/2000JB900188.

Lamont, T. N., Roberts, N. M. W., Searle, M. P., Gopon, P., Waters, D. J., & Millar, I. (2020). The age, origin, and emplacement of the Tsiknias Ophiolite, Tinos, Greece. Tectonics, 39, e2019TC005677. https://doi.org/10.1029/2019TC005677

Loher, M., Pape, T., Marcon, Y., Römer, M., Wintersteller, P., Praeg, D., ... & Bohrmann, G. (2018). Mud extrusion and ring-fault gas seepage–upward branching fluid discharge at a deep-sea mud volcano. Scientific reports, 8(1), 1-11.

Loreto, M. F., Zitellini, N., Ranero, C. R., Palmiotto, C., & Prada, M. (2020) Extensional tectonics during the Tyrrhenian back-arc basin formation and a new morpho-tectonic map.Basin Research. DOI: 10.1111/bre.12458

Maffione, M., & van Hinsbergen, D. J. J. (2018). Reconstructing plate boundaries in the Jurassic Neo-Tethys from the East and West Vardar Ophiolites (Greece and Serbia). Tectonics, 37, 858–887. https://doi.org/10.1002/2017TC004790

Malinverno, A., & Ryan, W. B. (1986). Extension in the Tyrrhenian Sea and shortening in the Apennines as result of arc migration driven by sinking of the lithosphere. Tectonics, 5(2), 227-245.

Manu-Marfo, D., Aoudia, A., Pachhai, S., & Kherchouche, R. (2019). 3D shear wave velocity model of the crust and uppermost mantle beneath the Tyrrhenian basin and margins. Scientific reports, 9(1), 3609.

Marroni, M., Meneghini, F., & Pandolfi, L. (2017). A Revised Subduction Inception Model to Explain the Late Cretaceous, Double-Vergent Orogen in the Precollisional Western Tethys: Evidence From the Northern Apennines.Tectonics,36(10), 2227-2249.

Mohn, G., Manatschal, G., Beltrando, M., & Haupert, I. (2014). The role of rift-inherited hyper-extension in Alpine-type orogens. Terra Nova, 26(5), 347-353.

Moghadam, H. S., & Stern, R. J. (2015). Ophiolites of Iran: Keys to understanding the tectonic evolution of SW Asia:(II) Mesozoic ophiolites. Journal of Asian Earth Sciences, 100, 31-59.https://doi.org/10.1016/j.jseaes.2014.12.016

Müller, R. D., Sdrolias, M., Gaina, C., & Roest, W. R. (2008). Age, spreading rates, and spreading asymmetry of the world's ocean crust. Geochemistry, Geophysics, Geosystems, 9(4). https://doi.org/10.1029/2007GC001743

Nicolosi, I., Speranza, F., & Chiappini, M. (2006). Ultrafast oceanic spreading of the Marsili Basin, southern Tyrrhenian Sea: Evidence from magnetic anomaly analysis. Geology,

34(9), 717-720.

Okay, A. I., Tuysuz, O., Satır, M., Ozkan-Altiner, S. E. V. İ. N. Ç., Altiner, D. E. M. İ. R., Sherlock, S., & Eren, R. H. (2006). Cretaceous and Triassic subduction-accretion, high-pressure–low-temperature metamorphism, and continental growth in the Central Pontides, Turkey. Geological Society of America Bulletin, 118(9-10), 1247-1269.

Pérez-Gussinyé, M., Ranero, C. R., Reston, T. J., & Sawyer, D. (2003). Mechanisms of extension at nonvolcanic margins: Evidence from the Galicia interior basin, west of Iberia. Journal of Geophysical Research: Solid Earth, 108(B5).

Pérez-Gussinyé, M., Morgan, J. P., Reston, T. J., & Ranero, C. R. (2006). The rift to drift transition at non-volcanic margins: Insights from numerical modelling.Earth and Planetary Science Letters,244(1-2), 458-473.

Piana-Agostinetti, N., Steckler, M. S., & Lucente, F. P. (2009). Imaging the subducted slab under the Calabrian Arc, Italy, from receiver function analysis. Lithosphere, 1(3), 131-138.

Polonia, A., Torelli, L., Mussoni, P., Gasperini, L., Artoni, A., & Klaeschen, D. (2011). The Calabrian Arc subduction complex in the Ionian Sea: Regional architecture, active deformation, and seismic hazard. Tectonics, 30(5).

Prada, M., Sallarès, V., Ranero, C. R., Vendrell, M. G., Grevemeyer, I., Zitellini, N., & de Franco, R. (2015). The complex 3-D transition from continental crust to backarc magmatism and exhumed mantle in the Central Tyrrhenian basin. Geophysical Journal International, 203(1), 63-78. doi: 10.1093/gji/ggv271

Prada, M., Ranero, C. R., Sallarès, V., Zitellini, N., & Grevemeyer, I. (2016). Mantle exhumation and sequence of magmatic events in the Magnaghi–Vavilov Basin (Central Tyrrhenian, Italy): new constraints from geological and geophysical observations. Tectonophysics, 689, 133-142.

Reston, T., & Manatschal, G. (2011). Rifted margins: Building blocks of later collision. In Arc-continent collision (pp. 3-21). Springer, Berlin, Heidelberg.

Schettino, A., & Turco, E. (2011). Tectonic history of the western Tethys since the Late Triassic. GSA Bulletin, 123(1-2), 89-105. https://doi.org/10.1130/B30064.1

Sharkov, E., Lebedev, V., Chugaev, A., Zabarinskaya, L., Rodnikov, A., Sergeeva, N., & Safonova, I. (2015). The Caucasian-Arabian segment of the Alpine-Himalayan collisional belt: Geology, volcanism and neotectonics. Geoscience Frontiers, 6(4), 513-522. https://doi.org/10.1016/j.gsf.2014.07.001

Schmid, S. M., Pfiffner, O. A., Froitzheim, N., Schönborn, G., & Kissling, E. (1996). Geophysical-geological transect and tectonic evolution of the Swiss-Italian Alps. Tectonics, 15(5), 1036-1064.

Spakman, W. and Wortel, R. (2004), A tomographic view on the Western Mediterranean Geodynamics, in: The TRANSMED Atlas, The Mediterranean Region from Crust to Mantle, Edited by: Cavazza, W., Roure, F., Spakman, W., Stamgli, G.M., Ziegler, P., pp.31-52

Stampfli, G. M., Mosar, J., Marquer, D., Marchant, R., Baudin, T., & Borel, G. (1998). Subduction and obduction processes in the Swiss Alps. Tectonophysics, 296(1-2), 159-204.

Wessel, P., & Smith, W. H. (1995). New version of the generic mapping tools. Eos, Transactions American Geophysical Union, 76(33), 329-329.

Wortel, M. J. R., & Spakman, W. (2000). Subduction and slab detachment in the Mediterranean-Carpathian region. Science, 290(5498), 1910-1917.

Vitale, S., Ciarcia, S., Fedele, L., & Tramparulo, F. D. A. (2019). The Ligurian oceanic successions in southern Italy: The key to decrypting the first orogenic stages of the southern Apennines-Calabria chain system. Tectonophysics, 750, 243-261.

Zelt, C. A., & Forsyth, D. A. (1994). Modeling wide-angle seismic data for crustal structure: Southeastern Grenville Province. Journal of Geophysical Research: Solid Earth, 99(B6), 11687-11704.

Zelt, C. A. (1998). Lateral velocity resolution from three-dimensional seismic refraction data. Geophysical Journal International, 135(3), 1101-1112.

Zitellini, N., Ranero, C. R., Loreto, M. F., Ligi, M., Pastore, M., D'Oriano, F., ... & Prada, M. (2020). Recent inversion of the Tyrrhenian Basin. Geology, 48(2), 123-127.

657

10 Figures

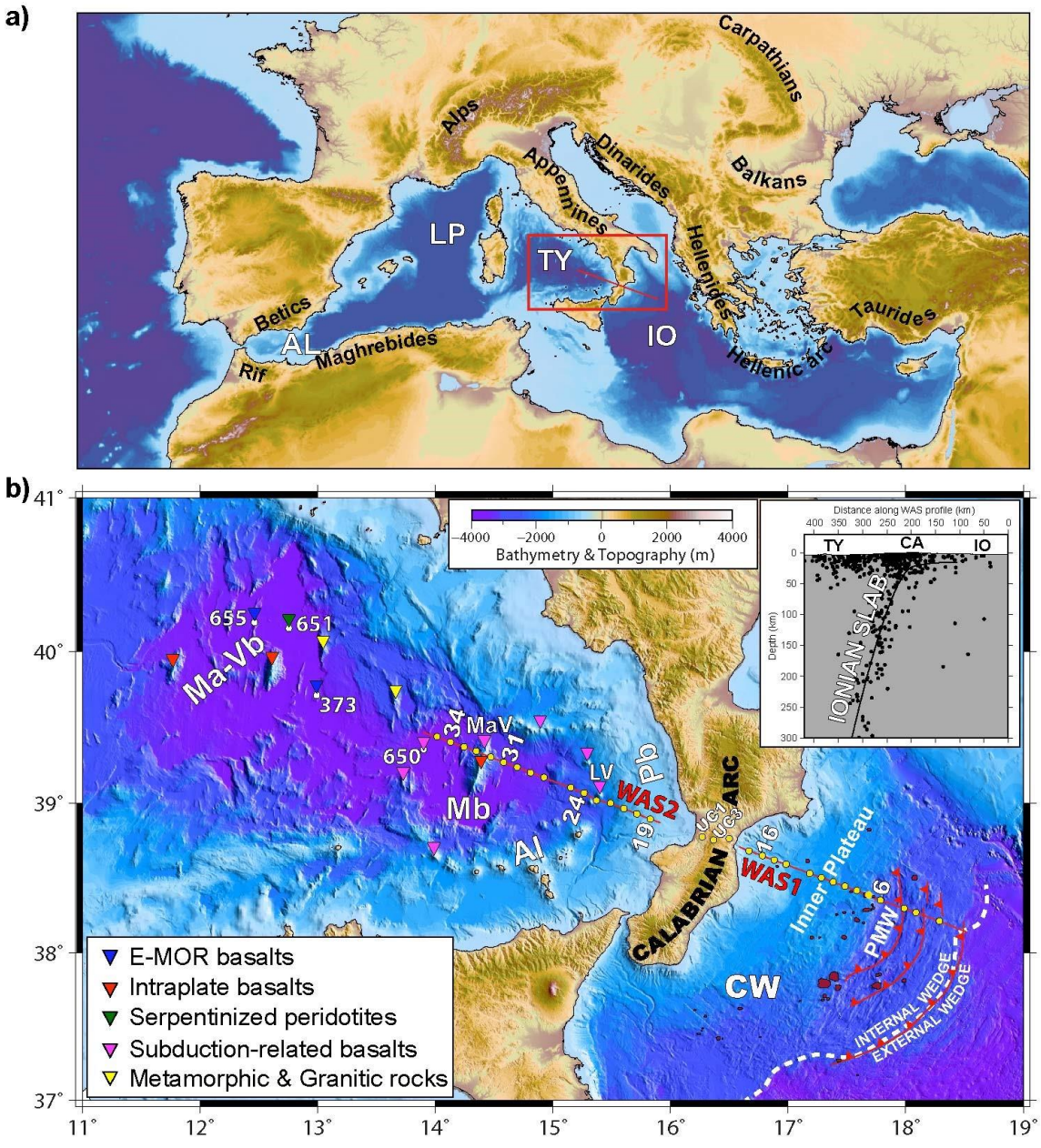

Figure 1. a) Bathymetry and topography map of the Mediterranean region showing the location of the main Cenozoic orogenic belts, and the location of the seismic cross section presented in this study. AL: Alboran Sea, LP: LP: Liguro-Provençal, TY: Tyrrhenian, IO: Ionian. b) Bathymetry map of the Tyrrhenian and Ionian region showing the petrological nature of basement rocks from ODP sites (Kastens and Mascle, 1990), DSDP sites (Dietrich et al., 1977), and dredging samples (Colantoni et al., 1981). Yellow circles

depict the location of ocean bottom seismometers and land stations used to record shots along profiles WAS 1 and WAS 2. The record sections of numbered OBSs and land stations UC1 and UC3 are shown in Figure 2. White circles show the location of ODP and DSDP boreholes in the Tyrrhenian, while mud volcanoes in the Contractional wedge (CW) are depicted with dark red circles. The boundary between the internal and external wedge (dashed white line) and the location of mud volcanoes is taken from Gutscher et al. (2017), and Loher et al. (2018), while the location of the morphological domains of the Inner plateau and the Pre-Messinian wedge (PMW) are taken from Polonia et al. (2011). Red lines and triangles in the PMW are splay faults from Polonia et al. (2011). Earthquakes occurring within ±50 km of distance from the WAS profile are projected along the geophysical cross section and presented in the small inset to show the steep (~70^{o}) geometry of the Ionian slab beneath the study area (earthquakes are from Chiarabba et al., 2005). AI: Aeolian Islands, CA: Calabria, LV: Lametini Volcano, Ma-Vb: Magnaghi-Vavilov basins, Mb: Marsili basin, MaV: Marsili Volcano, Pb: Paola basin.

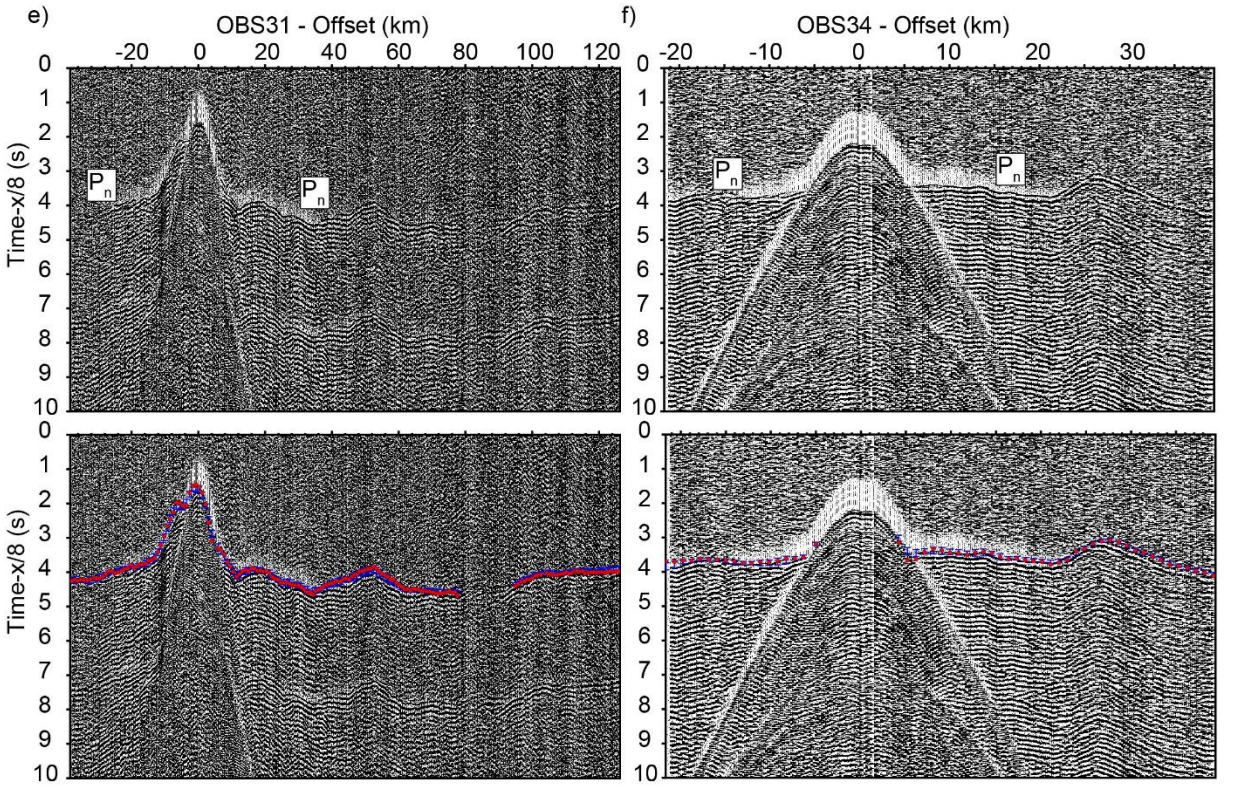
e)
OBS31 - Offset (km)
-20 0 20 40 60 80 100 120
Time-x/8 (s)
P_n
P_n
f)
OBS34 - Offset (km)
-20 -10 0 10 20 30
P_n
P_n

681

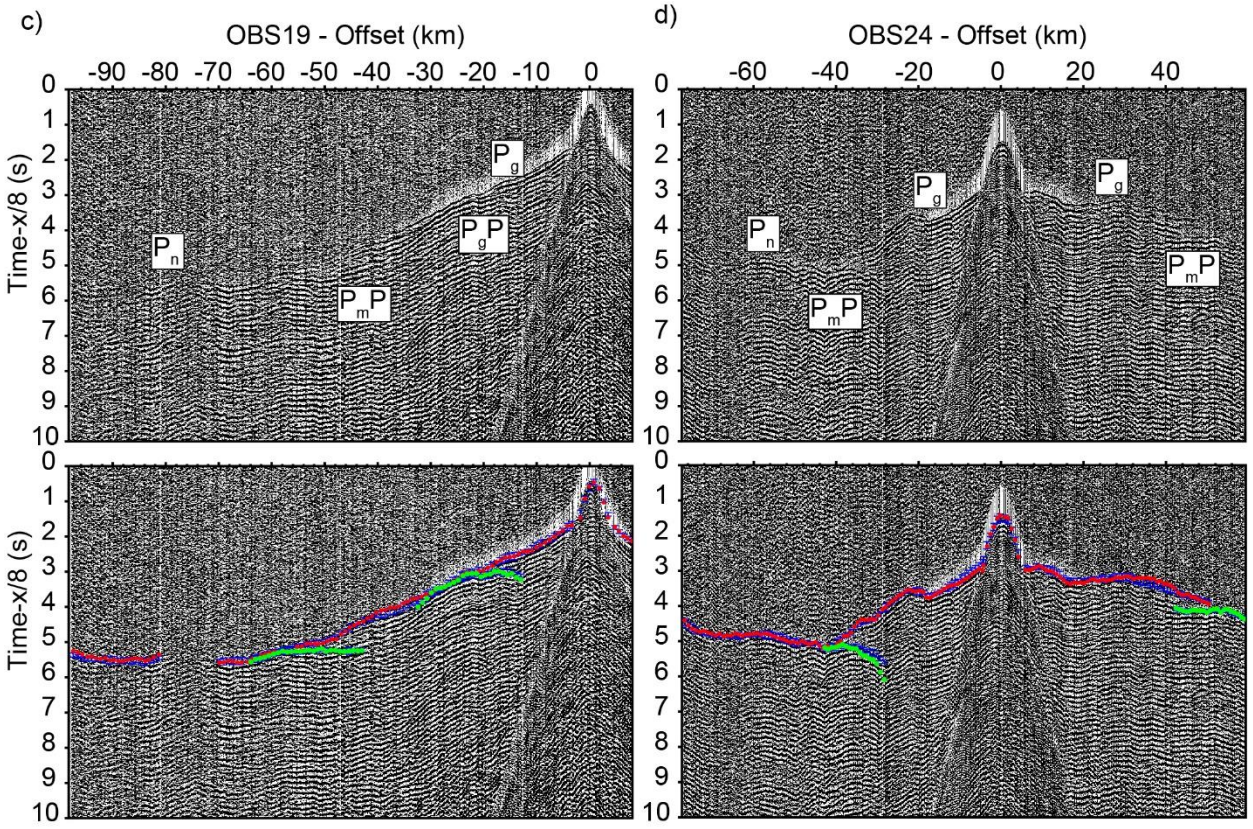
c)
OBS19 - Offset (km)
-90 -80 -70 -60 -50 -40 -30 -20 -10 0
Time-x/8 (s)
P_g
P_gP
P_n
P_mP
d)
OBS24 - Offset (km)
-60 -40 -20 0 20 40
P_g
P_g
P_g
P_n
P_mP
P_mP

682

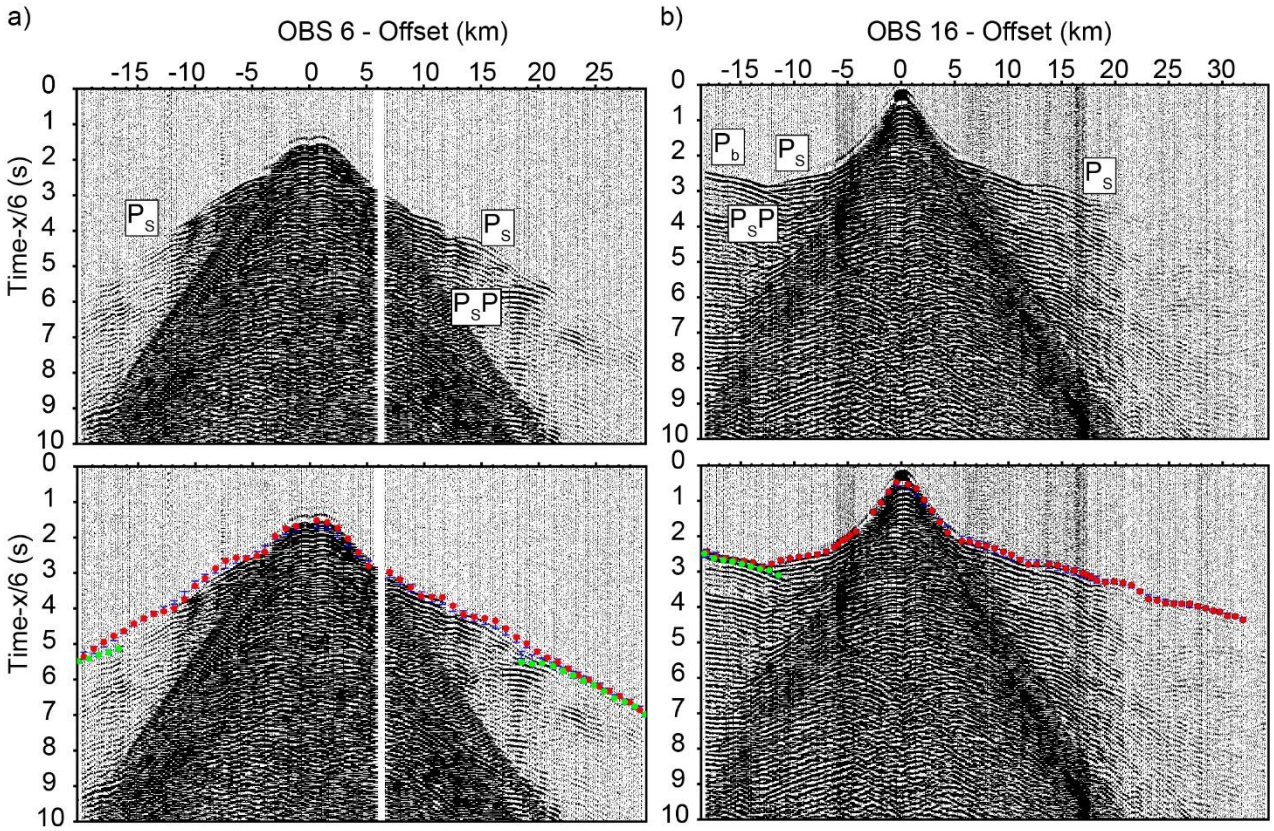
a)
OBS 6 - Offset (km)
-15 -10 -5 0 5 10 15 20 25
Time-x/6 (s)
0 1 2 3 4 5 6 7 8 9 10
P_S
P_S
P_SP
b)
OBS 16 - Offset (km)
-15 -10 -5 0 5 10 15 20 25 30
P_b
P_S
P_S
P_SP

683

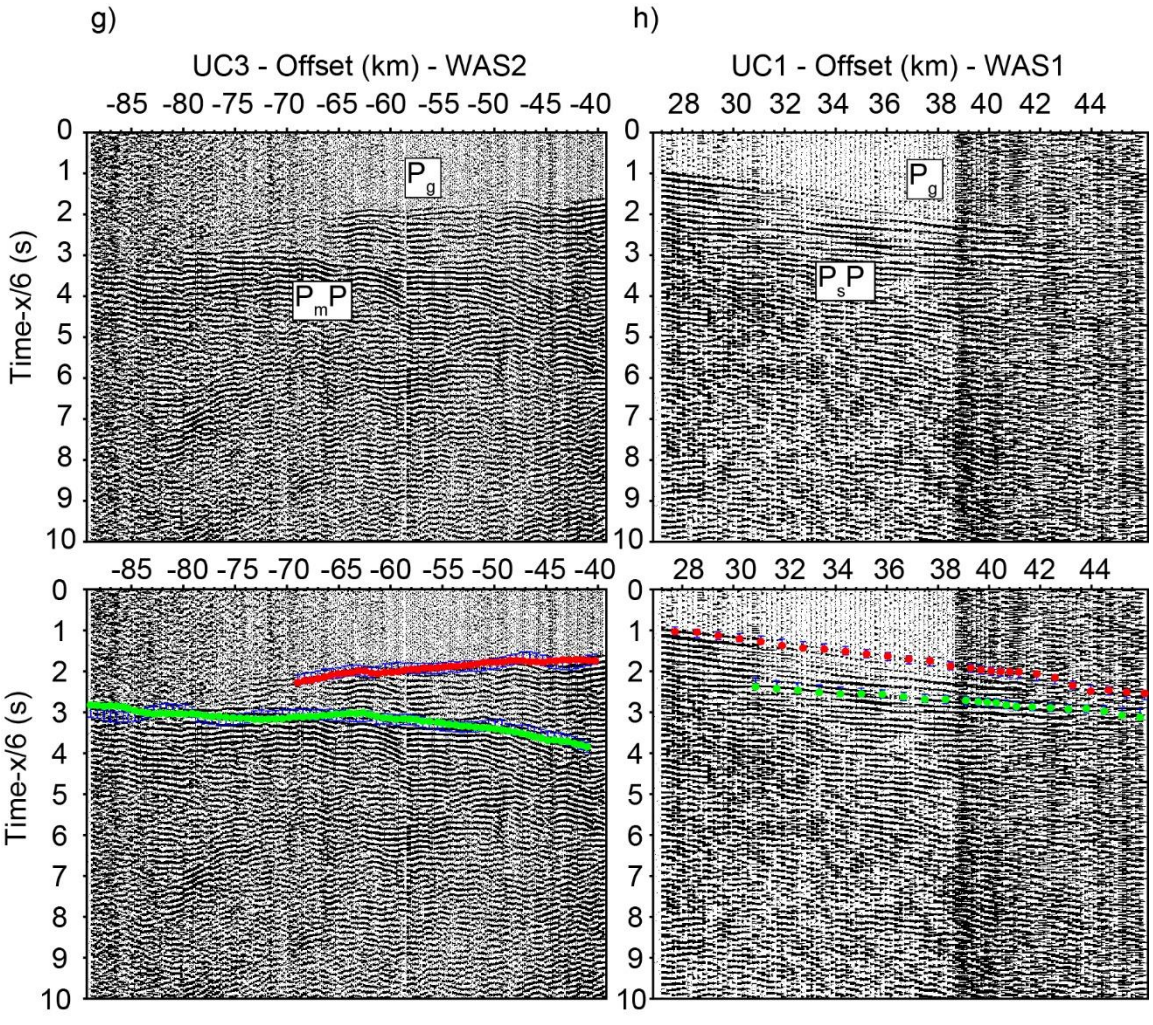

684

685 **Figure 2.** Seismic record sections of OBSs (a)6, (b)16, (c)19, (d)24, (e)31, (f)34, and land
686 station (g) UC3 record from profile WAS2, and (h) UC1 record from profile WAS1. The
687 location along the line of each instrument is shown in Fig. 1b. The upper panels show the
688 interpreted seismic phases, while the lower panels show the records with the picked
689 refraction and reflection travel-times (blue bars), and the corresponding synthetic
690 refraction (red dots) and reflection (green dots) travel-times obtained in the final model.

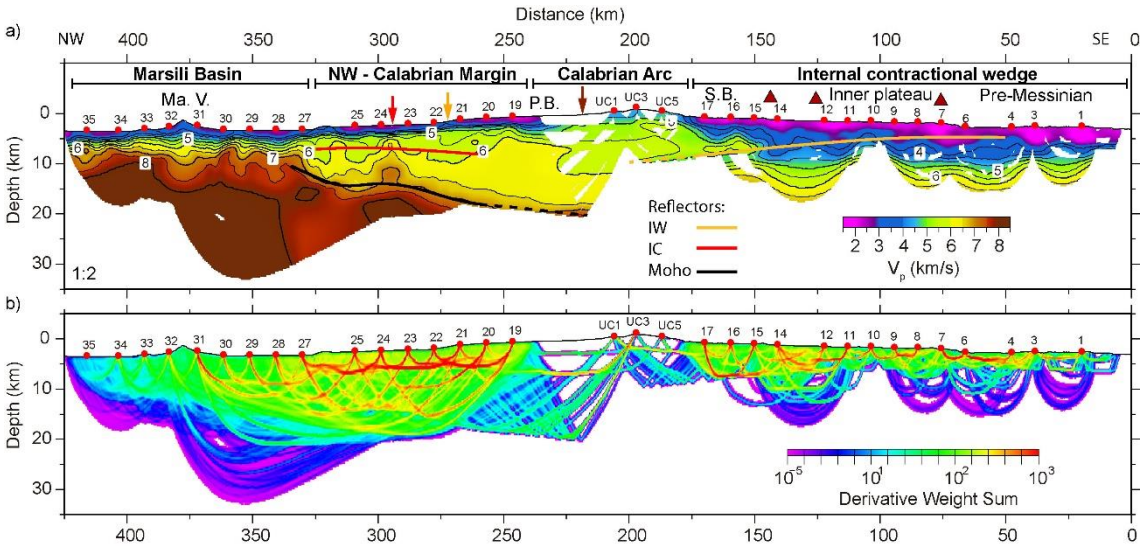

691

692 **Figure 3.** 2D P-wave velocity model of the Calabrian subduction system obtained from
693 joint inversion of refracted and reflected travel-times. The inverted reflectors are intra-
694 wedge reflector (IW), the intra-crustal interface (IC) and the Moho along the NW
695 Calabrian margin. Ma.V: Marsili Volcano, P.B: Paola basin S.B.: Squillace basin. Red
696 dots are OBS and land stations. Vertical red, orange, and brown arrows indicate the
697 location of the vertical velocity-depth profiles shown in Figure 7a. Red arrow also shows
698 the location of the volcanic arc, while the dark red triangle shows the location of mud
699 volcanism neighboring WAS line 1 in Fig. 1. (b) Derivative weight sum of the
700 tomographic model. This image can be used as a proxy for the refracted and reflected ray
701 coverage through the grid during the inversion.

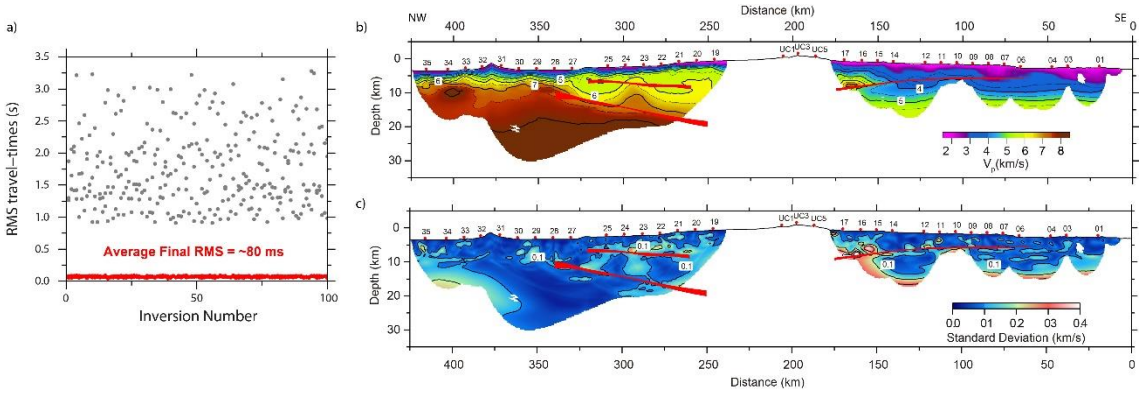

702

Figure 4. a) Distribution of RMS travel-times of the first (grey dots) and final (red dots) iteration of each Monte Carlo realization (100 in total) showing how the initial random distribution converges to a common solution (Final RMS ~80ms). b) Average final tomographic model of the 100 Monte Carlo final solutions. The red bands depict the error bar of each reflector. c) Standard deviation of the 100 realizations.

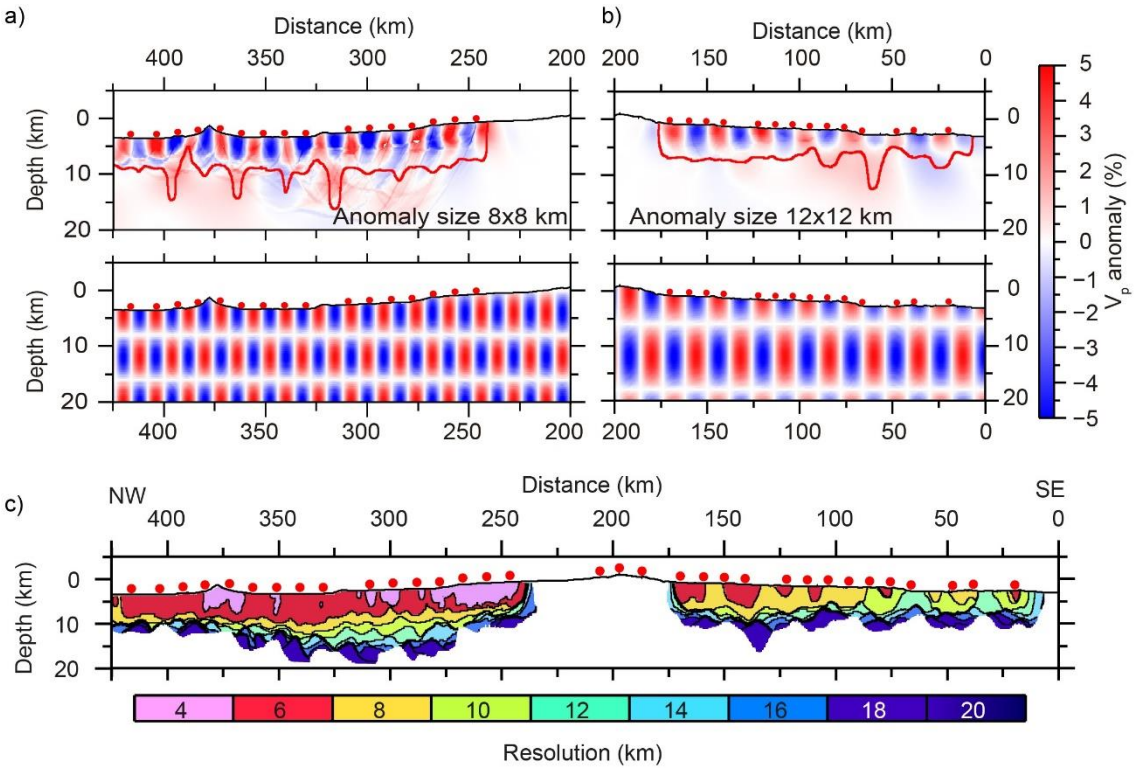

Figure 5. Retrieved (upper) and true (lower) checkerboard pattern of the (a) 8x8 km and (b) 12x12 km anomaly size. The red contour line indicates where the patter is retrieved satisfactorily (i.e. where the semblance is ~0.7). Red dots are OBSs. c) Resolution map of the model showing the region at which we are able to retrieve each size of the checkerboard pattern.

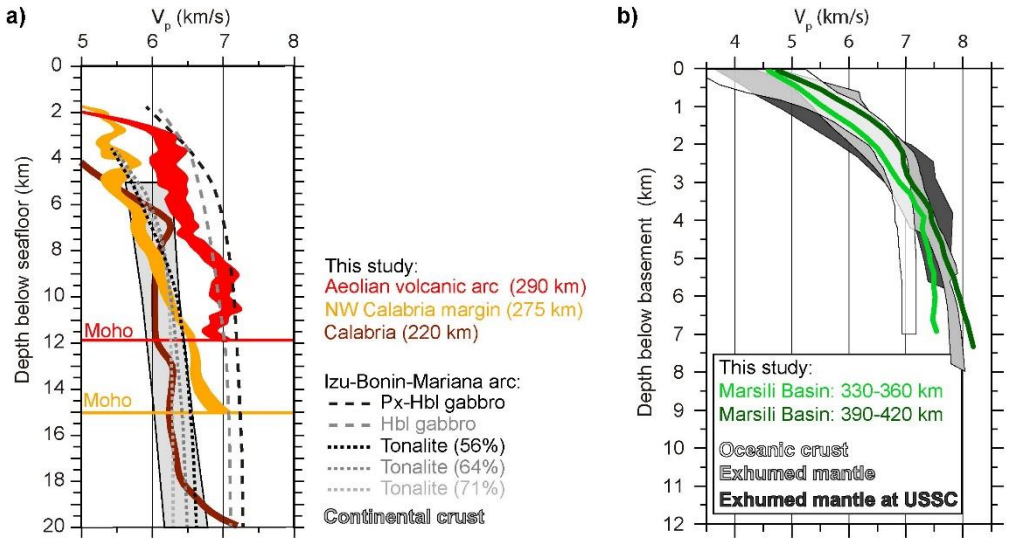

714

715 **Figure 6**. a) Velocity-depth profiles of the region of the volcanic arc (red band), the NW
716 Calabrian margin (yellow band), and mainland Calabria (dark brown) compared with the
717 continental crust velocity-depth function of Christensen and Mooney (1995) and the
718 velocity-depth function for tonalitic and gabbroic rocks of the Izu-Bonin-Mariana arc
719 (Kitamura et al., 2003). The thickness of each profile from our model corresponds to the
720 error bars inferred from the Monte Carlo analysis. Note that no error bar is drawn for the
721 Calabrian profile as the Monte Carlo analysis was focused on the offshore regions. b)
722 Average velocity-depth profiles of the NW (light green) and SE (dark green) Marsili
723 volcanic area compared with the velocity-depth reference function for oceanic crust from
724 Grevemeyer et al. (2018a), and exhumed mantle regions of the Tyrrhenian and the Gulf
725 of Cadiz from Prada et al. (2015), and at ultra-slow spreading centers (USSC)
726 Grevemeyer et al. (2018b).

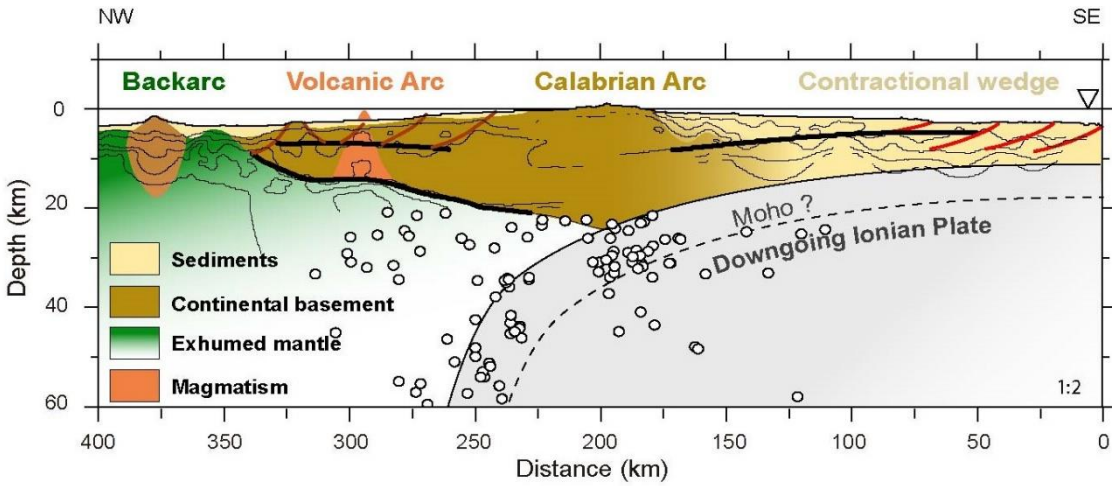

727

728 **Figure 7.** Interpretative cross section of the entire Calabrian subduction system based on
729 the result of this study and the depth-distribution of earthquakes from 20 to 60 km of
730 depth (white circles) from Fig. 1b. The geometry of the Ionian subducting slab is taken
731 from (Chiarabba et al., 2005), while the Ionian oceanic Moho is based on the results from
732 Cassinis et al. (2003) and Piana-Agostinetti et al. (2009). Brown lines delineate
733 interpreted normal faults along the NW Calabrian margin, while red lines are
734 compressional features across the Inner plateau and the Pre-Messinian wedge observed
735 by Polonia et al. (2011). Thick black lines are wide-angle seismic boundaries constrained
736 by the tomographic model in this study. Thin black lines are isovelocity contours shown
737 in Fig. 3.